Correlation Analysis of SFI Peculiar Velocities

Stefano Borgani
Istituto Nazionale de Fisica Nucleare

Luiz N. da Costa
European Southern Observatory

Idit Zehavi
Fermi National Accelerator Laboratory

Riccardo Giovanelli
Cornell University

Martha P. Haynes
Cornell University

See next page for additional authors

Authors

Stefano Borgani, Luiz N. da Costa, Idit Zehavi, Riccardo Giovanelli, Martha P. Haynes, Wolfram Freudling, Gary Wegner, and John J. Salzer

CORRELATION ANALYSIS OF SFI PECULIAR VELOCITIES

STEFANO BORGANI

Istituto Nazionale de Fisica Nucleare, Sezione di Trieste, c/o Dipartimento di Astronomia dell'Università, via Tiepolo 11, I-34100 Trieste, Italy; and Istituto Nazionale di Fisica Nucleare, Sezione di Perugia

LUIZ N. DA COSTA

European Southern Observatory, Karl-Schwarzschild-Strasse 2, D-85748 Garching bei München, Germany; and Observatório Nacional, Rua General José Cristino 77, 20921-400 São Cristovão, RJ, Brazil

IDIT ZEHAVI

NASA Fermilab Astrophysics Group, Fermi National Accelerator Laboratory, Box 500, Batavia, IL 60510

RICCARDO GIOVANELLI AND MARTHA P. HAYNES

Center for Radiophysics and Space Research and National Astronomy and Ionosphere Center,[1] Cornell University, Ithaca, NY 14953

WOLFRAM FREUDLING

Space Telescope European Coordinating Facility, European Southern Observatory, Karl-Schwarzschild-Strasse 2, D-85748 Garching bei München, Germany

GARY WEGNER

Department of Physics and Astronomy, Dartmouth College, Hanover, NH 03755

AND

JOHN J. SALZER

Department of Astronomy, Wesleyan University, Middletown, CT 06459

Received 1999 May 3; accepted 1999 August 12

ABSTRACT

We present results of a statistical analysis of the SFI catalog of peculiar velocities, a recently completed survey of spiral field galaxies with *I*-band Tully-Fisher distances. The velocity field statistic utilized is the velocity correlation function, $\psi_1(r)$, originally introduced by Górski et al. The analysis is performed in redshift space so as to circumvent potential ambiguities connected with inhomogeneous Malmquist bias corrections. The results from the SFI sample are compared with linear-theory predictions for a class of cosmological models. We generate a large set of mock samples, extracted from *N*-body simulations, which are used to assess the reliability of our analysis and to estimate the associated uncertainties. We assume a class of cold dark matter–like power spectrum models, specified by σ_8, the rms fluctuation amplitude within a sphere of $8\ h^{-1}$ Mpc radius, and by the shape parameter, Γ. Defining $\eta_8 = \sigma_8 \Omega_0^{0.6}$, we find that the measured $\psi_1(r)$ implies a degenerate constraint in the (η_8, Γ)-plane, with $\eta_8 = 0.3 \pm 0.1(\Gamma/0.2)^{0.5}$ at the $2\ \sigma$ level for the inverse Tully-Fisher (ITF) calibration presented in this paper. We investigate how much this constraint changes as we account for uncertainties in the analysis method and uncertainties in the distance indicator, and we consider alternative ITF calibrations. We find that both changing the error-weighting scheme and selecting galaxies according to different limiting line widths has a negligible effect. On the contrary, the model constraints are quite sensitive to the ITF calibration. The other ITF calibrations, by Giovanelli et al. and da Costa et al. both yield, for $\Gamma = 0.2$, a best-fit value of $\eta_8 \simeq 0.6$.

Key words: cosmology: observations — cosmology: theory — galaxies: distances and redshifts — large-scale structure of universe

1. INTRODUCTION

The peculiar velocity field of galaxies provides a very powerful way of probing mass fluctuations on intermediate to large scales ($\lesssim 100\ h^{-1}$ Mpc, *h* being the Hubble constant in units of 100 km s^{-1} Mpc^{-1}), as it is sensitive primarily to large-scale density fluctuations. Therefore, studies of cosmic flows can be used to constrain the amplitude of the large-scale mass power spectrum, thus complementing the information on intermediate scales, between those probed by redshift surveys and those sampled by anisotropies in the cosmic microwave background as observed by *COBE* (see the review by Dekel 1994). Another advantage in studying the velocity field is that it is measured on scales for which linear approximation to gravitational instability is expected to hold, thus allowing one to explore more thoroughly the parameter space of cosmological models. We can parameterize the fluctuation power spectrum in terms of the rms fluctuation within spheres of $8\ h^{-1}$ Mpc, σ_8, and of a shape parameter Γ. Then, according to linear theory, the typical amplitude of the peculiar velocity on a given scale is proportional to $\eta_8 f(\Gamma, R)$, where $\eta_8 = \sigma_8 \Omega_m^{0.6}$ (following the notation of Chiu, Ostriker, & Strauss 1998, Ω_m here is the matter density parameter) and $f(\Gamma, R)$ is a quantity that depends on the power spectrum shape and on the scale R at which the velocity field is probed.

Several statistical characterizations of the peculiar velocity fields have been proposed in the last decade with the aim of providing more robust constraints on cosmological scenarios as newer and larger data sets have come to completion (see, e.g., Strauss & Willick 1995 for a review).

Among such statistical measures, in this paper we will concentrate on the velocity correlation function, which has been introduced for turbulence studies by Monin & Yaglom (1975) and borrowed for cosmology by Peebles (1980; see also Górski 1988). We will apply this statistic to the SFI sample, a recently completed homogeneous all-sky survey of Sbc–Sc galaxies with I-band Tully-Fisher (T-F) distances (Giovanelli et al. 1997a; Haynes et al. 1999a, 1999b, hereafter H99a and H99b, respectively).

A first application of the velocity correlation statistic to observational data was realized by Górski et al. (1989, hereafter G89; see also Groth, Juszkiewicz, & Ostriker 1989), who analyzed the spiral galaxy sample by Aaronson, Huchra, & Mould (1979) and the elliptical galaxy sample by Burstein et al. (1987), finding substantial discrepancies between the results obtained from these two data sets. Tormen et al. (1993, hereafter T93) analyzed the correlation statistics of the Mark II sample, with results favoring $\eta_8 \simeq 0.7$ for scale-invariant cold dark matter (CDM) models. Kolatt & Dekel (1996) estimated the matter power spectrum implied by the POTENT reconstruction of the Mark III data (Willick et al. 1997) and found $\eta_8 \simeq 0.7$–0.8. More recently, maximum likelihood (ML) analyses, estimating the mass power spectrum that gives rise to the observed peculiar velocities, have been performed by Zaroubi et al. (1997) on the Mark III sample and by Freudling et al. (1999, hereafter FZ99) on the SFI sample. Both analyses consistently find $\eta_8 \simeq 0.8 \pm 0.2$ (90% confidence level), quite independent of the power spectrum shape. These results point toward high-amplitude fluctuations and thus are somewhat at variance with results from the rms cluster peculiar velocity (e.g., Borgani et al. 1997; Watkins 1997) and with constraints from the local cluster abundance (e.g., Eke, Cole, & Frenk 1996; Girardi et al. 1998), which indicate lower values.

Studies of the peculiar velocity can also be combined with analyses of all-sky redshift surveys to investigate the relation between the galaxy and underlying mass distributions, a key ingredient for understanding galaxy biasing. Comparisons between the measured peculiar velocities or the recovered densities with those predicted from all-sky redshift surveys are commonly used to estimate the parameter $\beta = \Omega_m^{0.6}/b$, under the assumption of linear biasing with a bias factor b. Several estimates of β have been presented in the literature (e.g., da Costa et al. 1998, hereafter dC98; Willick & Strauss 1998; Branchini et al. 1999 and references therein), based on comparisons between the velocity fields directly inferred from T-F data and recovered from the galaxy density field in the *IRAS* 1.2 Jy (Fisher et al. 1995) and the PSCz surveys. Such analyses generally find β-values in the range 0.5–0.7. Taking $b = \sigma_{8,\text{IRAS}}/\sigma_8$, these results would imply $\eta_8 \simeq 0.35$–0.50 for $\sigma_{8,\text{IRAS}} \simeq 0.7$ (Fisher et al. 1994). On the other hand, analyses based on the comparison of density fields provide values of β as large as 0.9 (e.g., Sigad et al. 1998). The interpretation of the β-values is further complicated if galaxy biasing is better described by a stochastic, nonlinear process (e.g., Dekel & Lahav 1999).

The aim of this paper is to perform a detailed analysis of the velocity correlation function for the SFI sample and to derive the resulting constraints on large-scale structure formation models. The comparison with theoretical expectations is based on linear-theory predictions, and we resort to large-scale N-body simulations to verify the reliability of our analysis and to estimate the associated errors contrib-

uted by both the cosmic variance and by the scatter in the T-F relation.

In our analysis, we choose to use redshift-space information as the indicator of distance for the SFI galaxies, so as to avoid the associated Malmquist bias arising from the intrinsic scatter of the distance indicator when using the inferred distances (see Freudling et al. 1995, for a discussion on bias corrections in the SFI sample). The forward T-F relation obtained by regressing the apparent magnitudes over the line width, in this case, is still susceptible to selection bias due to the imposed magnitude limit. Using the inverse relation, i.e., fitting the line width as a function of the apparent magnitude, avoids this selection bias as long as the sample selection is independent of the line width (see § 6 of Strauss & Willick 1995, and references therein). For this reason, we perform our analysis in redshift space by using peculiar velocities estimated from the inverse Tully-Fisher (ITF) relation.

The outline of the paper is as follows: In § 2, we provide a basic description of the SFI sample and present the ITF calibrations on which our analysis is based. Section 3 contains a brief introduction to the velocity correlation formalism and presents the results of its application to the SFI data. In § 4, we present the velocity correlation analysis of our mock samples. In § 5, we derive the resulting constraints on cosmological models and discuss the impact of systematic effects in both the sample definition and the correlation analysis method. We summarize our main conclusions in § 6.

2. SFI SAMPLE

The T-F data defining the sample used here consist of two main data sets: (1) a subset of the Mathewson, Ford, & Buchhorn (1992) survey with about 1200 galaxies with I-band photometry and measured rotational velocities, either from radio observations of 21 cm line widths or optical rotation curves, and (2) the SFI I-band T-F redshift-distance survey of about 1300 Sbc–Sc field galaxies. The SFI sample consists of galaxies with inclination $\gtrsim 45°$ north of $\delta = -45°$ and Galactic latitudes $|b| > 10°$. The original Mathewson et al. (1992) measurements of magnitude and rotational velocities were converted to the SFI system using about 200 to 300 common galaxies.

In addition to the field galaxies, roughly 800 galaxies covering a broader range of morphological types were observed in the field of 24 clusters (Giovanelli et al. 1997a, 1997b, hereafter G97; SCI sample). After careful membership assignment, cluster galaxies were used to derive a combined T-F relation corrected for Malmquist bias and bias introduced by incompleteness and different morphological mix. To perform our analysis in redshift space, we consider the ITF relation between the absolute magnitude, M, and the full line width, W,

$$M = a + b(\log W - 2.5), \qquad (1)$$

with $a = -20.95$ and $b = -7.94$ (here W is expressed in units of km s^{-1}, and we assume a Hubble constant of 100 km s^{-1} Mpc^{-1}). This relation has the same slope as that originally provided by G97, whose zero point, $b = -21.10$, is 0.15 mag smaller. This difference is due to a new determination of the velocity widths and to the removal of 71 galaxies for poor photometry, poor line widths, or obvious misidentification (cf. H99a, H99b). The 1 σ uncertainty in the zero point has been estimated by G97 to be about 0.05

mag when combining statistical uncertainties in the T-F fitting and uncertainties in defining the cluster reference frame with a finite number (24) of such objects. This uncertainty does not, however, include possible systematics associated with the processing of the raw data, with the difference between the T-F relation of clusters and field galaxies, or with potential deviations of our local universe from a global Hubble flow (e.g., Zehavi et al. 1998; but see also Giovanelli et al. 1999).

We note that careful analysis of the T-F relation for galaxies in clusters suggests that the scatter depends on the line width. This dependence is modeled by letting the error in the estimated distance r_i of the ith galaxy be $\epsilon_i = \Delta(W_i)r_i$, where $\Delta(W_i)$ is the fractional error in the distance as estimated from the scatter about the ITF relation as a function of the measured line width of the galaxy (G97; see also Willick et al. 1997 and Willick & Strauss 1998). The resulting errors are estimated to be in the range 15%–20%.

Unless otherwise specified and following da Costa et al. (1996) and FZ99, we discard those ($\sim 7\%$) SFI galaxies with line width log $W \leq 2.25$ because of the limited reliability of the ITF relation at such line widths. We will also show the robustness of the final results against changes in the assumed limiting line width. Furthermore, we restrict our analysis to the SFI subsample defined by galaxies lying within $cz \leq 6000$ km s^{-1}. With such restrictions, the final sample on which we base our analysis contains 974 galaxies.

A further alternative calibration of the ITF relation has been presented by dC98, based on a comparison of the velocity field of the SFI sample and that implied by the IRAS 1.2 Jy survey. The resulting zero point and slope of the ITF relation are $a = -21.11$ and $b = -8.55$, respectively. In the following, we will use the above most recent ITF calibration as the reference but will show the effect of taking the previous G97 and dC98 calibrations on the final constraints on cosmological parameters.

3. VELOCITY CORRELATION STATISTICS

The estimator for the velocity correlations that we will use in the following is that introduced by G89 and is given by

$$\psi_1(r) = \frac{\sum_{|\mathbf{r}_i - \mathbf{r}_j| = r} w_i w_j u_i u_j \cos \vartheta_{ij}}{\sum_{|\mathbf{r}_1 - \mathbf{r}_j| = r} w_i w_j \cos^2 \vartheta_{ij}}, \qquad (2)$$

where ϑ_{ij} is the angle between the direction of the ith and the jth galaxy and the sums are over all the galaxy pairs at separation r in redshift space. With the above definition, the $\psi_1(r)$ statistic is independent of any assumptions regarding the velocity field, such as homogeneity and isotropy, and has been shown by G89 to be rather robust to sampling fluctuations. In equation (2), u_i is the radial peculiar velocity of the ith galaxy and w_i represents a suitable weight to be assigned to it. The introduction of the weights is a slight modification of the expression for ψ_1 provided by G89 (see also T93). The following different weighting schemes will be applied: (1) uniform weighting, $w_i = 1$, (2) weighting galaxies according to their distance error, $w_i = 1/\epsilon_i$, and (3) weighting according to $w_i^2 = 1/(\epsilon_i^2 + \sigma_f^2)$, where σ_f^2 is the variance of the local velocity field.

The quantity σ_f can be interpreted as a line-of-sight velocity dispersion and has been introduced to model possible nonlinearities, which generate small-scale random motions within virialized regions. Such motions, which

would give rise to an uncorrelated velocity component, are expected to be relatively unimportant for the SFI field galaxies, whose peculiar velocity should not be much affected by virial motions. A further possible interpretation of σ_f is an unrecognized distance-independent error, which is not accounted for by the ITF scatter calibrated by using members of distant clusters (e.g., Kaiser 1988). FZ99 checked for such a term by having it as a another degree of freedom to be constrained by a maximum likelihood approach and found $\sigma_f = 200 \pm 120$ km s^{-1}. When resorting to weighting scheme 3, we will take $\sigma_f = 150$ km s^{-1}, although our final results are essentially insensitive to its choice.

As for scheme 1, its main drawback is that it assigns the same weight to all objects, regardless of the uncertainty in the velocity errors, which increase with distance. Although schemes 2 and 3 overcome this limitation, they reduce the effective sampling volume and have been shown by Dekel, Bertschinger, & Faber (1990) to overestimate the contribution of well-sampled regions with respect to undersampled regions in the reconstruction of velocity fields. In the following, we will mainly base our analysis on the uniform weighting scheme, which is the least affected by cosmic scatter (see § 4 below).

As shown by G89, the ensemble average of $\psi_1(r)$ is given by

$$\Psi_1(r) = \langle \psi_1(r) \rangle = \mathscr{A}(r)\Psi_\parallel(r) + [1 - \mathscr{A}(r)]\Psi_\perp(r), \quad (3)$$

under the assumption of homogeneity and isotropy, where $\Psi_\parallel$ and $\Psi_\perp$ are the radial and transverse correlation functions of the three-dimensional peculiar velocity field. In linear theory, they are connected to the power spectrum of density fluctuations, $P(k)$, according to

$$\Psi_\parallel(r) = \frac{f(\Omega_m)^2 H_0^2}{2\pi^2} \int dk\, P(k) \left[j_0(kr) - 2\frac{j_1(kr)}{kr} \right],$$

$$\Psi_\perp(r) = \frac{f(\Omega_m)^2 H_0^2}{2\pi^2} \int dk\, P(k) \frac{j_1(kr)}{kr}, \qquad (4)$$

where $j_i(x)$ is the ith-order spherical Bessel function and $f(\Omega_m) \simeq \Omega_m^{0.6}$.

The quantity $\mathscr{A}$ appearing in equation (3) is a moment of the selection function of the sample depending on the spatial distribution of galaxies according to

$$\mathscr{A}(r) =$$

$$\frac{\sum_{|\mathbf{r}_i - \mathbf{r}_j| = r} w_i w_j [r_i r_j(\cos \vartheta_{ij} - 1) + r^2 \cos \vartheta_{ij}] \cos \vartheta_{ij}}{r^2 \sum_{|\mathbf{r}_i - \mathbf{r}_j| = r} w_i w_j \cos^2 \vartheta_{ij}}. \quad (5)$$

This quantity provides in a sense the relative contribution to $\psi_1(r)$ from the radial and transverse components of the velocity correlation. The definition of equation (5) is slightly different from that previously adopted by other authors, by including the galaxy weights.

The advantage of using ψ_1 is that it can be directly calculated from the observed radial velocities, without the need of any additional assumption. It can then be related to theory (eqs. [3]–[4]), taking into account the specific sampling through equation (5). The geometric factor $\mathscr{A}(r)$ is plotted in Figure 1 for the three mentioned weighting schemes. The net effect of nonuniform weighting is that of increasing $\mathscr{A}(r)$ at separations $\gtrsim 2000$ km s^{-1}. This is the consequence of the fact that $\Psi_\perp$ takes relatively more con-
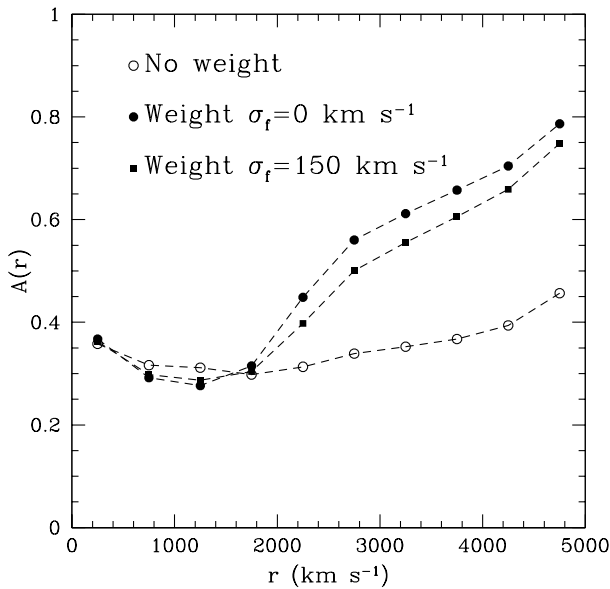
FIG. 1.—The geometric factor $\mathscr{A}(r)$ (eq. [5]; see text), associated with the SFI sample, for the three alternative weighting schemes.

tribution than $\Psi_\parallel$ from large-scale fluctuations (see, e.g., Górski 1988). Therefore, its contribution to $\Psi_1(r)$ is suppressed with the error weighting, which amounts to decreasing the effective volume of the sample.

The velocity correlation function $\psi_1(r)$ for the SFI sample, with the H99 calibration, computed within bins of 500 km s^{-1}, is plotted in Figure 2. No error bars are assigned here to $\psi_1(r)$. We will discuss in § 4.3 how to associate uncertainties to model predictions to provide confidence levels (CLs) in the estimate of cosmological parameters. The upper panel shows the effect of adopting different weighting schemes. It is apparent that the choice for w_i has a marginal impact on the correlation signal. This result might seem somewhat unexpected, in view of the different $\mathscr{A}(r)$ values
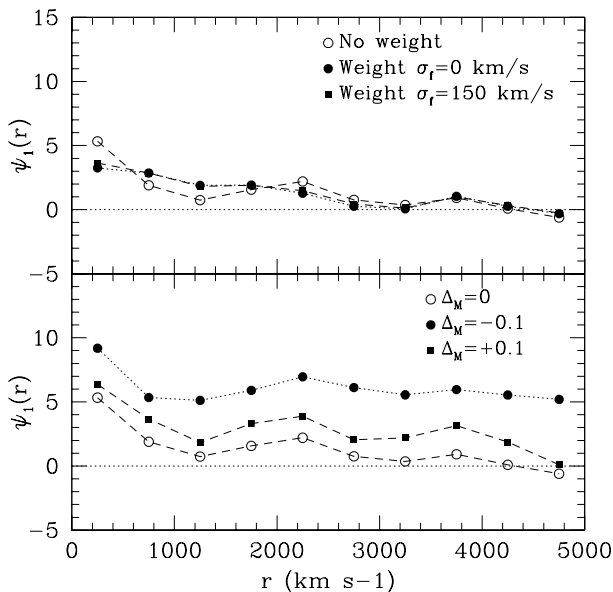

FIG. 2.—The velocity correlation function, $\psi_1(r)$ (in units of 10^4 km s^{-1}), for the SFI sample. *Top*, effect of different galaxy weights; *bottom*, effect of changing by 0.1 mag the zero point of the ITF relation, representing the 2 σ uncertainty in its calibration (cf. G97; H99a, H99b).

for the weighted and unweighted cases. However, these differences appear only at rather large separations, $r \gtrsim 2000$ km s^{-1} (cf. Fig. 1), where the value of ψ_1 for SFI rapidly declines, thus making any difference among different weighting schemes hardly detectable. By comparing this result with that from the real-space analysis of the Mark II sample by T93, it turns out that the SFI sample produces a velocity correlation signal that is at least a factor of 2 smaller, although the corresponding scales at which $\psi_1(r)$ approaches zero ($\simeq 3000$ km s^{-1}) are similar.

The lower panel of Figure 2 shows the effect of changing the zero point of the ITF relation (eq. [1]) by 0.1 mag either way, which corresponds to a change of $\epsilon \sim 2.5\%$ in the distances or an additional global Hubble-like flow ϵr. This change corresponds to the 2 σ formal statistical uncertainty estimated from the analysis of the SCI sample of cluster galaxies (G97; H99a, H99b). A global Hubble-like flow represents a coherent velocity field that is characterized by a positive correlation (i.e., galaxies moving in the same direction) on intermediate scales ($r \lesssim 5000$ km s^{-1}) and by a negative correlation at the largest scales ($r \gtrsim 7000$ km s^{-1}), when the two galaxies of a pair are placed in the opposite directions of the sample.

Alternative estimators of the velocity correlation statistics have been applied by different authors. Groth et al. (1989; see also Kaiser 1988) considered the generic form for the velocity correlation tensor under the assumption of a homogeneous and isotropic velocity field, $\Psi_{ij}(r) = \langle v_i(\mathbf{x}) v_j(\mathbf{x} - \mathbf{r}) \rangle = \Psi_\perp(r) \delta_{ij} + [\Psi_\parallel(r) - \Psi_\perp(r)] \hat{r}_i \hat{r}_j$, where δ_{ij} is the Kronecker delta. Then they obtained $\Psi_\perp$ and $\Psi_\parallel$ by a χ^2 minimization procedure to the data. G89 compared this method with their $\psi_1(r)$ approach and showed that they produce comparable results, although the former turns out to be noisier at large separations, $r \gtrsim 4000$ km s^{-1}.

More recently, Ferreira et al. (1999) proposed a new method to estimate the main galaxy pairwise velocity, $v_{12} = \langle v(\mathbf{x}_1) - v(\mathbf{x}_2) \rangle$. This method, which has been so far tested on N-body mock samples and is in the process of being applied to real data sets, provides essential constraints on $\sigma_8^2 \Omega_m^{0.6}$. Therefore, its combination with linear-theory constraints on $\sigma_8 \Omega_m^{0.6}$ could in principle break the degeneracy between σ_8 and Ω_m. Of course, careful investigations are required to understand whether available data are of sufficient quality and whether their systematics and biases are under control enough to allow a reliable estimate of σ_8 and Ω_m separately.

4. ANALYSIS OF MOCK SAMPLES

To explore the model parameter space extensively, we resort in the following to linear theory as the means to compare model predictions and SFI results. Two important issues need to be addressed: (1) the reliability of our analysis and, specifically, the use of linear theory to predict the statistics of the velocity field and (2) the estimate of the cosmic scatter and the observational uncertainties associated with the SFI sampling to establish the confidence level for model exclusion. For this purpose, we use large N-body simulations from which we extract sets of mock samples that mimic the sampling and selection effects of the SFI sample.

4.1. *Generating the Mock Samples*

The parent N-body simulations from which we extract mock samples have been run by using the publicly available adaptive P^{3}M code by Couchman (1991). We have run two

simulations corresponding to two different cosmological scenarios. The first model is a flat, low-density one with $\Omega_m = 0.4$ (Λ0.4). The transfer function used is that of Bardeen et al. (1986) (see eq. [7] below), with the shape parameter, Γ, set to 0.22, and $\sigma_8 = 0.87$. The second model is an Einstein–de Sitter (EdS) universe, with $\Gamma = 0.43$ and $\sigma_8 = 1.2$. With the above parameters, both models are consistent with the 4 year *COBE* normalization (e.g., Bunn & White 1997), while the EdS model fails to match the abundance of local galaxy clusters (e.g., Eke et al. 1996; Girardi et al. 1998) and the shape of the galaxy power spectrum (e.g., Peacock & Dodds 1994; Liddle et al. 1996).

Each simulation follows 128^3 particles within a box 250 h^{-1} Mpc on a side. The adopted Plummer softening scale, $\simeq 100\ h^{-1}$ kpc, is more than adequate to describe the large-scale velocity field (see Borgani et al. 1999 for a more detailed description of the simulations). Velocity fields on scales of a few tens of h^{-1} Mpc, which are of interest in this paper, receive a small but nonnegligible contribution from wavelengths larger than the adopted box size. Furthermore, the volume of a single simulation can accommodate only a rather small number of nonoverlapping SFI mock samples (each extending out to $cz = 6000$ km s^{-1}), so as not to allow a reliable determination of cosmic variance.

To extend the dynamic range of our simulations to larger scales, we resorted to the method proposed by Tormen & Bertschinger (1996), adding longer waves to N-body outputs. This method, which allows us to generate nonperiodic replicas of a parent box, is based on the Zeldovich (1970) approximation for computing the contribution to particle displacements and velocities from waves longer than the original box size. Cole (1997) showed that this procedure is adequate to extend to larger scales the description of peculiar velocities. In our analysis, we replicate the original box three times along each spatial direction, which leads to a total of 27 replicas and a final box of size $L = 750$ h^{-1} Mpc, containing about 5.7×10^7 particles.

As a first step for mock sample extraction, we divide the large box into 6^3 smaller boxes of 125 h^{-1} Mpc on a side. At the center of each of them we place an "observer." After randomly choosing the orientation of the "galactic" coordinate system, we select among the simulation particles those that are closest to the position of real galaxies in the SFI sample. In this way, we generate mock samples with the same spatial distribution and number of galaxies as in the real SFI sample. The "true" radial velocities in the mock samples are perturbed according to the associated observational errors of the real catalog and according to the assumed random velocity dispersion σ_f (under the assumption that both contributions are independent Gaussian variables). For each simulation, we generate two sets of mock samples, based on assuming both $\sigma_f = 0$ and 150 km s^{-1}. Since the final results turn out to be essentially indistinguishable, we will present for the mock sample analysis only results based on assuming a vanishing σ_f.

We note that other authors (e.g., G89; Strauss, Cen, & Ostriker 1993; T93) followed more sophisticated procedures to search for "observers" within simulations. Such procedures involve selecting observers so that local properties of the density and velocity field resemble those observed for the Local Group of galaxies. However, T93 showed that applying such constraints on the observer selection does not significantly alter the velocity correlation statistics for realistic power spectra. Furthermore, the aim of our analysis

is to estimate how often the SFI correlation statistics can be observed in a given cosmology, assuming the variety of observers' characteristics are included in the cosmic variance that is appropriate for that model.

4.2. *Testing the Analysis Method*

Since the mock samples have been generated by reproducing the positions of real galaxies, their corresponding $\mathscr{A}(r)$ is the same as for the real SFI sample. For each cosmological model, we compute in linear theory the expected ψ_1 (eq. [3]) and compare it with the distribution of values obtained from the mock samples using equation (2). We plot in Figure 3 the results of this comparison for the Λ0.4 case, for both uniform (*top*) and distance-error (*bottom*) weightings. Circles represent $\psi_1(r)$ as estimated by averaging over the set of $N_{\mathrm{mock}} = 216$ model samples, and the error bars indicate the 1 σ scatter, arising from both cosmic variance and observational uncertainties. As a basic result, it turns out that for both weighting schemes linear theory is always adequate to describe the expected velocity correlation function for samples having the same selection effects as the SFI, once they are accounted for by the $\mathscr{A}(r)$ quantity. Any residual discrepancy on small ($\lesssim 1500$ km s^{-1}) scales, which is probably due to sampling effects or to residual nonlinearities, is well within the 1 σ scatter. Furthermore, we also recall that, since the SFI sample contains only field spirals, we expect their dynamics to be even closer to linear theory than that of the N-body particles belonging to the mock samples, and therefore we did not attempt to select, so as to avoid high-density regions.

We checked the relative contribution to the errors from the cosmic scatter and from the uncertainties in the peculiar velocity measurements, using a set of mock samples in which peculiar velocities are not perturbed according to ITF distance errors, so that only the effect of the cosmic scatter is present. It turns out that the cosmic scatter is clearly dominant at $r < 3500$ km s^{-1}, with the T-F scatter
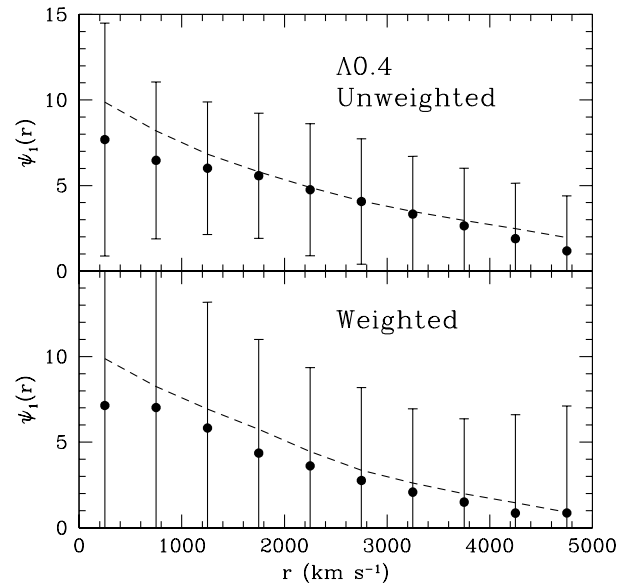

FIG. 3.—Comparison between linear-theory predictions (*dashed curves*) and results from the analysis of mock samples for the velocity correlation function $\psi_1(r)$ (in units of 10^4 km s^{-1}). Mock samples are extracted from an N-body simulation of the Λ0.4 model. *Top*, uniform weighting; *bottom*, distance-error weighting. Error bars indicate the 1 σ scatter among the set of 216 mock samples.

contributing more than 20% and becoming relevant only at larger scales. The distance-error weighting scheme generates a larger scatter, because this method amounts to reducing the effective volume where $\psi_1(r)$ is computed. For this reason, in the following we will take the uniform weighting as the reference analysis method to constrain model parameters.

4.3. Estimating ψ_1 Uncertainties

Having demonstrated that linear theory provides reliable predictions for ψ_1, the next information that one needs is the uncertainty to be associated to such predictions. To do so, we estimate from the set of mock samples the elements of the covariance matrix, C^{ij}, which are defined as

$$C^{ij} = \frac{1}{N_{\text{mock}}} \sum_{l=1}^{N_{\text{mock}}} (\psi_{1,l}^i - \bar{\psi}_1^i)(\psi_{1,l}^j - \bar{\psi}_1^j) . \tag{6}$$

Here $\psi_{1,l}^i$ is the value of the velocity correlation function at the ith separation bin for the lth mock sample, while $\bar{\psi}_1^i$ is its average value estimated over the N_{mock} samples.

Figure 4 shows the comparison between results from the $\Lambda0.4$ and EdS models by plotting the quantities $C^{ij}/\psi_1^i \psi_1^j$. According to its definition, this quantity describes the relative covariance of the ψ_1 values at different separations. The top panels show the results for the diagonal (variance) terms, while the other panels show the off-diagonal terms, illustrating different rows in the covariance matrix. The first thing to note is the large cross-correlation between the results of the different bins, which are comparable to the variances and, therefore, cannot be ignored when using the ψ_1 statistic to constrain cosmological models.

In addition, it is apparent from Figure 4 that, apart from small differences due to statistical fluctuations, the two models have the same amount of relative covariance. This is not unexpected, since to a first approximation, the long-wave perturbations, which generate the cosmic scatter, are also responsible for the ψ_1 signal, so as to make the relative scatter fairly constant. Noticeable differences occur only at relatively large separations, more than 3500 km s^{-1}, where the observational uncertainties become more dominant, thus increasing the total scatter and suppressing the discriminative power of $\psi_1(r)$. For this reason, in the following we will compare linear-theory predictions and SFI results only for $r \leq 3500$ km s^{-1}, where the relative uncertainties are essentially the same for the two considered models. We note that, since $\Lambda0.4$ and EdS have rather different values for both η_8 and for the power spectrum shape, we can quite confidently conclude that the relative scatter for $\psi_1(r)$ is model independent, at least for the range of models and scales of interest, while its absolute value is not.

In the top right panel of Figure 4, we compare the diagonal terms for the $\Lambda0.4$ mock samples for ψ_1 computed according to uniform weighting and distance-error weighting schemes. It is apparent that the distance-error weighting is associated with larger error bars, as was already shown in Figure 3.
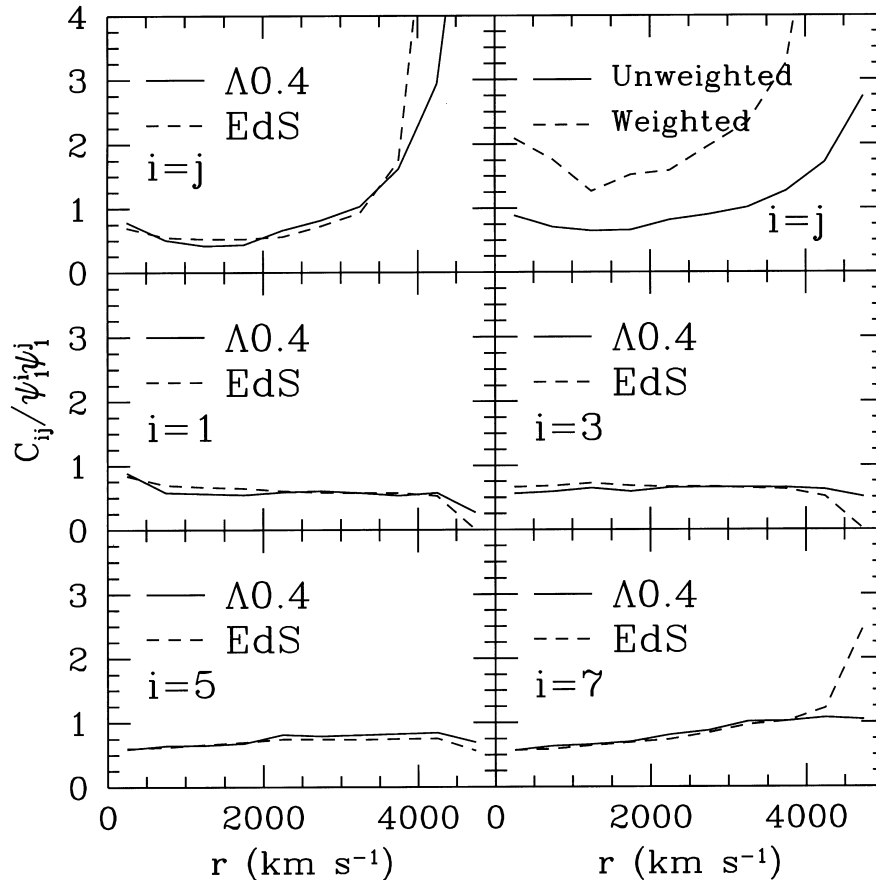

FIG. 4.—Elements of the relative covariance matrix, $C^{ij}/\psi_1^i \psi_1^j$, for SFI mock samples extracted from EdS and $\Lambda0.4$ simulations. *Top panels*, diagonal (variance) terms; *top right*, comparison of the variance for unweighted and error-weighted estimates of $\psi_1(r)$; *other panels*, off-diagonal terms, showing different rows in the covariance matrix (see text).

Based on these results, therefore, we conclude that (1) the errors of individual ψ_1 bins are significantly correlated; (2) a general recipe can be devised for the ψ_1 uncertainties, whose relative amount is fairly independent of the cosmological model; and (3) the size of such errors is smaller when ψ_1 is estimated according to the uniform-weighting scheme.

5. CONSTRAINING COSMOLOGICAL MODELS

Based on the results obtained so far, we will now use equations (3) and (4) as a model prediction for ψ_1. As for the model power spectrum, we express it as $P(k) = AkT^2(k)$ where we assume a Harrison-Zeldovich shape on large scales. The transfer function, $T(k)$, is taken to be

$$T(q) = \frac{\ln(1 + 2.34q)}{2.34q}$$
$$\times \left[1 + 3.89q + (16.1q)^2 + (5.46q)^3 + (6.71q)^4\right]^{-1/4},$$

$$(7)$$

where $q = k/\Gamma h$ and Γ is the so-called shape parameter. For $\Gamma \simeq \Omega_m h$, equation (7) provides the transfer function for CDM models with a negligible baryon fraction (Bardeen et al. 1986). More generally, it can be seen as a phenomenological expression, with Γ a parameter to be fixed by observational constraints. As for the amplitude of the power spectrum, it is customary to express it in terms of σ_8. Following equation (4), the velocity correlation function $\psi_1(r)$ is then entirely specified in linear theory by the two parameters Γ and η_8.

Despite the error bars being so large such that the ψ_1 detection is only marginally different from zero in each individual bin (cf. Figs. 2 and 3), its determination at different scales does allow us to place significant constraints on the (η_8, Γ)-plane. To provide constraints on these parameters, we compute the weighted χ^2 between the SFI correlation function, ψ_1^{SFI}, and that from model predictions, ψ_1^{mod}:

$$\chi^2 = \sum_{i,j} [\psi_1^{SFI}(r_i) - \psi_1^{mod}(r_i)]C_{ij}^{-1}[\psi_1^{SFI}(r_i) - \psi_1^{mod}(r_i)] . \quad (8)$$

Here C_{ij}^{-1} are the elements of the inverse of the covariance matrix, as calibrated from the mock samples, and the sums are over the radial bins of 500 km s^{-1} width, for separations $r \leq 3500$ km s^{-1}. The probability for model rejection is estimated by assuming a χ^2 statistic, from the value of $\Delta\chi^2 = \chi^2 - \chi^2_{min}$, where χ^2_{min} is the absolute minimum value.

In Figure 5, we plot the iso-$\Delta\chi^2$ contours for the three ITF calibrations of the SFI sample that were discussed in § 2. Internal and external contours correspond to $\Delta\chi^2 = 2.30$ and 6.17, respectively, thus providing the 1 σ and 2 σ confidence levels for two significant parameters. The corresponding minimum values of the χ^2 per degree of freedom are 1.67, 0.80, and 0.78, for the H99, G97, and dC98 calibrations, respectively. In all cases, the best-fitting model seems to provide an acceptable fit. This value for the H99 calibration is somewhat large; however, it corresponds to only ~1 σ deviation for a χ^2 statistic with five degrees of freedom. The fact that such χ^2 values are around unity indicates that our error model is realistic.

The hatched vertical areas represent the 95% confidence level interval on the shape parameter, as derived by Liddle et al. (1996) from the power spectrum of APM galaxies. The hatched horizontal areas represent the 90% confidence level on η_8 derived by Borgani et al. (1997) from an analysis of
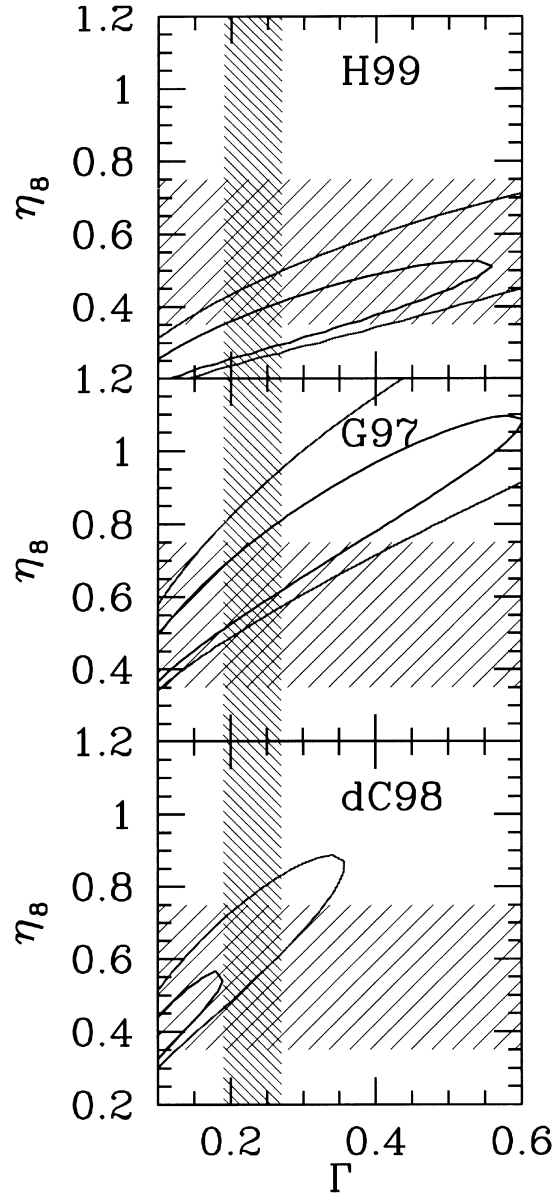

FIG. 5.—The 1 σ and 2 σ contours in the (η_8, Γ)-plane from the analysis of the velocity correlation function, $\psi_1(r)$, for different calibrations of the inverse Tully-Fisher relation. *Horizontal area*, 90% confidence level constraints on η_8 from the analysis of the Giovanelli et al. (1997a) and G97 rms cluster peculiar velocities (Borgani et al. 1997); *vertical area*, 95% confidence level constraint on the shape parameter from the power spectrum of APM galaxies (Liddle et al. 1996).

the rms peculiar velocity of SCI clusters (Giovanelli et al. 1997a; G97). All these constraints intersect our 2 σ confidence regions.

For the H99 and G97 ITF calibrations, the constraints in the (η_8, Γ)-plane can be cast in the form

$$\eta_8 = \eta_{8,0}(\Gamma/0.2)^{0.5} , \quad (9)$$

with $\eta_{8,0} = 0.30^{+0.12}_{-0.07}$ and $\eta_{8,0} = 0.58^{+0.22}_{-0.12}$ for the two above calibrations, respectively (error bars correspond to 2 σ CL). The asymmetry in the errors is due to the fact that, as η_8 is increased from its best-fitting values, larger absolute errors are assigned to ψ_1, since the relative scatter is taken

to be constant (cf. § 4.3). Thus, larger values of η_8 tend to be excluded at a lower significance than smaller values. As for the dC98 calibration, the corresponding constraints show a somewhat steeper Γ-dependence of η_8 with values of $\Gamma \gtrsim 0.35$ ruled out at about 2 σ CL. It is interesting to note that, for $\Gamma \simeq 0.2$, this result agrees with $\beta = 0.6 \pm 0.1$, as found by da Costa et al. (1998) for an almost unbiased *IRAS* galaxy distribution.

We show in Figure 6 the variation of $\Delta\chi^2$ around its minimum as a function of η_8, to show the effect of changing other assumptions underlying our analysis. In both panels, the solid curve refers to constraints from the H99 ITF calibration, for a fixed shape parameter $\Gamma = 0.2$ and $\log W > 2.25$ for the line width of SFI galaxies. As demonstrated already (Fig. 2, *top*), our results are insensitive to the choice of galaxy weighting, and we adopt here throughout the uniform weighting. As is illustrated in Figure 6b, changing the limiting line width of the sample also has a negligible effect on our results, which are virtually unchanged as we increase the line width from 2.25 to 2.40. We find as well that our constraints do not depend on the specific choice of binning used in the computation of $\psi_1(r)$. The effect of the zero-point uncertainty is shown in Figure 6a. As was illustrated also in the lower panel of Figure 2, the results are quite sensitive to such changes, and a negative shift of the ITF zero point by 0.1 mag leads to a sizeable increase of η_8 from $\simeq 0.3$ to $\simeq 0.55$. For higher values of Γ, this change would similarly correspond to higher values of η_8, e.g., for $\Gamma = 0.4$, η_8 would increase from $\simeq 0.4$ to $\simeq 0.8$, and its effect is generally comparable to that of varying the ITF calibration.

Despite the fact that the constraints on cosmological parameters drawn from the ψ_1 statistic are quite sensitive to the details of the ITF calibrations, some conclusions can still be drawn. First, the constraints on the velocity power spectrum normalization, η_8, depend on the $P(k)$ shape, as a consequence of the fact that we are probing velocity fields on scales larger than the 8 h^{-1} Mpc normalization scale. Second, assuming $\Gamma \simeq 0.2$, as indicated by galaxy clustering

data, implies power-spectrum amplitudes that can be different by up to a factor of 2 but are still generally consistent with independent observational constraints. For instance, the local abundance of galaxy clusters to a first approximation also provides a constraint on $\eta_8 = 0.5$–0.6 (e.g., Eke et al. 1996; Girardi et al. 1998 and references therein).

Our results for η_8 can also be compared with those obtained by Zaroubi et al. (1997) and FZ99, who estimated the mass power spectrum by an ML analysis of the peculiar velocities of the Mark III and the SFI samples, respectively. These estimates are then translated to constraints on η_8 by integrating over the corresponding spectra. Both works consistently found $\eta_8 \simeq 0.8 \pm 0.2$ at 90% CL and a preferred value of $\Gamma \simeq 0.4 \pm 0.2$. As the application of the ML analysis for the SFI sample has been performed using the G97 calibration, it is most suitable to compare the FZ99 results with those reported in the central panel of Figure 5. It turns out that the confidence regions coming from the ML and ψ_1 analyses do overlap over a significant portion of the (η_8, Γ)-plane. For $\Gamma = 0.4$, the ψ_1 analysis yields $\eta_8 = 0.85^{+0.17}_{-0.10}$, the main difference being the dependence of the η_8 constraints on Γ in the ψ_1 analysis, such that for lower values of $\Gamma \simeq 0.2$ the preferred η_8 values are somewhat smaller than those obtained in the ML analysis.

One should also bear in mind the different sensitivities of these two analyses. As demonstrated in Figures 5 and 6, the ψ_1 analysis is sensitive to the ITF calibration, while it is robust to changing the limiting line width. On the other hand, the ML analysis is remarkably robust to changes in T-F calibration (e.g., Fig. 8 in FZ99), while it is more sensitive to the pruning of SFI galaxies at different line widths. For these reasons, these two methods should be regarded as complementary and both worthy to be applied to a given data set.

6. CONCLUSION

In this paper, we have presented an analysis of the velocity correlation function, $\psi_1(r)$, for the SFI sample of Sbc–Sc
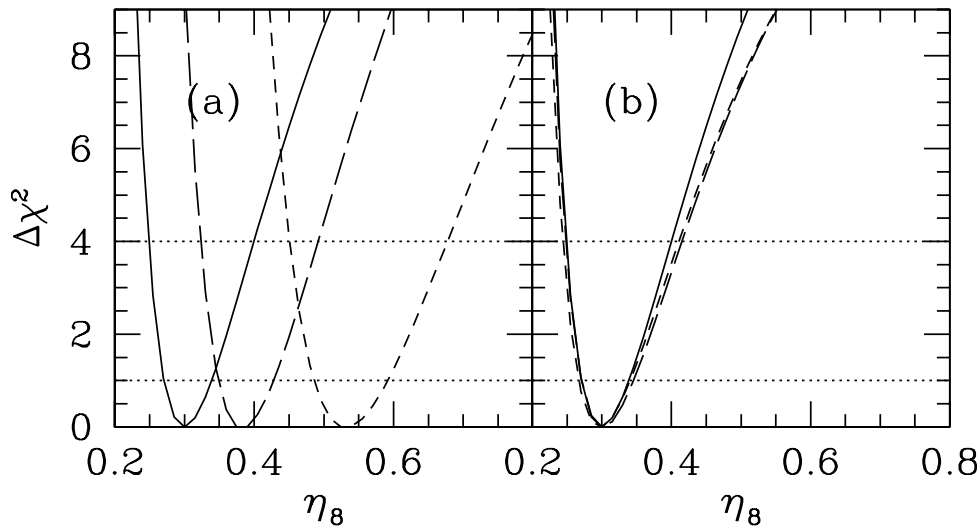

FIG. 6.—Variation of $\Delta\chi^2$ around its minimum value as a function of η_8. *Solid curves*: $\Gamma = 0.2$, uniform weighting in the estimate of $\psi_1(r)$, ITF calibration by H99a and H99b, with the best-fitting value of the zero point, and $\log W > 2.25$ for the galaxy line width. (*a*) Effect of changing the zero point of the ITF relation, shifting by 0.1 mag upward (*short-dashed lines*) and downward (*long-dashed lines*). (*b*) Effect of increasing the limiting line width. *Short-dashed lines*, $\log W > 2.3$; *long-dashed lines*, $\log W > 2.4$.

galaxy peculiar velocities based on the T-F distance indicator calibrated using a sample of cluster galaxies (Giovanelli et al. 1997a; G97; H99a, H99b). To minimize uncertainties related to Malmquist bias corrections, we performed the analysis using the redshift-space positions of galaxies and the ITF distance indicator. Three different ITF calibrations for the SFI sample have been examined in our analysis: that based on an updated version of the SFI sample presented by H99a and H99b, that presented by G97, and that obtained by dC98.

The final goal of our analysis is to place constraints on the amplitude and the shape of the fluctuation power spectrum by comparing $\psi_1(r)$ from SFI and from linear-theory predictions of cosmological models. For this purpose, we needed to verify the reliability of linear theory to predict $\psi_1(r)$ for a sample having the same galaxy positions and observational uncertainties as the SFI one and to estimate the associated uncertainties due to cosmic scatter and observational uncertainties. These two goals have been achieved by comparing linear-theory predictions with results from the analysis of a large set of mock SFI samples extracted from N-body simulations.

We have found that linear theory provides a rather accurate description of the $\psi_1(r)$ estimated from the mock samples over the whole scale range considered ($r \leq 5000$ km s^{-1}; see Fig. 3). This confirms that both sparse sampling effects and residual nonlinearities have a minor impact on our analysis. We have also shown that the relative covariance in $\psi_1(r)$ among the set of mock samples is roughly independent of the cosmological models, thus allowing for a simple treatment of the associated errors.

In general, we find that our analysis constrains a degenerate ridge in the (η_8, Γ)-plane. For the H99 and G97 ITF calibrations, we find $\eta_8 = \eta_{8,0}(\Gamma/0.2)^{0.5}$, with $\eta_{8,0} = 0.30^{+0.12}_{-0.07}$ and $\eta_{8,0} = 0.58^{+0.22}_{-0.12}$ for the two above calibrations, respectively, at the 2 σ level (cf. Fig. 5). The dC98

exhibits a stronger tendency for lower values of the shape parameter, constraining $\Gamma \lesssim 0.35$ at the 2 σ level and is consistent with the G97 calibration in that range. These constraints are robust to variations of the galaxy weighting scheme (see Fig. 2) and to changes in the choice of the limiting galaxy line width (see Fig. 6) but are, clearly, very sensitive to uncertainties in the calibration details, such as the zero point of the T-F relation.

In any case, the results presented here indicate that the large-scale velocity field can be brought into agreement with the low fluctuation amplitude implied at $\sim 10\ h^{-1}$ Mpc scale by the abundance of galaxy clusters (e.g., Eke et al. 1996; Girardi et al. 1998) for power spectrum shapes that are consistent with large-scale clustering data (e.g., Liddle et al. 1996), while higher amplitudes are allowed for larger values of the shape parameter. Our constraints on the (η_8, Γ)-plane for the ITF G97 calibration and those from the ML analysis for the G97 direct T-F relation by FZ99 are quite consistent for $\Gamma \gtrsim 0.3$. Since the ML and the ψ_1 methods are sensitive to different degrees to different aspects of the analysis (i.e., T-F calibration and limiting line width), they should be regarded as complementary approaches for extracting cosmological constraints from large-scale cosmic flows.

REFERENCES

Aaronson, M., Huchra, J., & Mould, J. R. 1979, ApJ, 229, 1
Bardeen, J. M., Bond, J. R., Kaiser, N., & Szalay, A. S. 1986, ApJ, 304, 15
Borgani, S., da Costa, L. N., Freudling, W., Giovanelli, R., Haynes, M. P., Salzer, J., & Wegner, G. 1997, ApJ, 482, L121
Borgani, S., Rosati, P., Tozzi, P., & Norman, C. 1999, ApJ, 517, 40
Branchini, E., et al. 1999, MNRAS, 308, 1
Bunn, E. F., & White, M. 1997, ApJ, 480, 6
Burstein, D., Davies, R. L., Dressler, A., Faber, S. M., Stone, R. P. S., Lynden-Bell, D., Terlevich, R. J., & Wegner, G. A. 1987, ApJS, 64, 601
Chiu, W. A., Ostriker, J. P., & Strauss, M. A. 1998, ApJ, 494, 479
Cole, S. 1997, MNRAS, 286, 38
Couchman, H. M. P. 1991, ApJ, 368, 23
da Costa, L. N., Freudling, W., Wegner, G., Giovanelli, R., Haynes, M. P., & Salzer, J. J. 1996, ApJ, 468, L5
da Costa, L. N., Nusser, A., Freudling, W., Giovanelli, R., Haynes, M. P., Salzer, J. J., & Wegner, G. 1998, MNRAS, 299, 425 (dC98)
Dekel, A. 1994, ARA&A, 32, 371
Dekel, A., Bertschinger, E., & Faber, S. M. 1990, ApJ, 364, 349
Dekel, A., & Lahav, O. 1999, ApJ, 520, 24
Eke, V. R., Cole, S., & Frenk, C. S. 1996, MNRAS, 282, 263
Ferreira, P. G., Juszkiewicz, R., Feldman, H. A., Davis, M., & Jaffe, A. H. 1999, ApJ, 515, L1
Fisher, K. B., Davis, M., Strauss, M. A., Yahil, A., & Huchra, J. P. 1994, MNRAS, 266, 50
Fisher, K. B., Huchra, J. P., Strauss, M. A., Davis, M., Yahil, A., & Schlegel, D. 1995, ApJS, 100, 69
Freudling, W., da Costa, L. N., Wegner, G., Giovanelli, R., Haynes, M. P., & Salzer, J. J. 1995, AJ, 110, 920
Freudling, W., et al. 1999, ApJ, 523, 1 (FZ99)
Giovanelli, R., Dale, D. A., Haynes, M. P., Hardy, E., & Campusano, L. E. 1999, ApJ, 525, 25
Giovanelli, R., Haynes, M. P., Herter, T., Vogt, N. P., Wegner, G., Salzer, J. J., da Costa, L. N., & Freudling W. 1997a, AJ, 113, 22
Giovanelli, R., Haynes, M. P., Herter, T., Vogt, N. P., da Costa, L. N., Freudling, W., Wegner, G., & Salzer, J. J. 1997b, AJ, 113, 53 (G97)

Girardi, M., Borgani, S., Giuricin, G., Mardirossian, F., & Mezzetti, M. 1998, ApJ, 506, 45
Gòrski, K. 1988, ApJ, 332, L7
Gòrski, K., Davis, M., Strauss, M. A., White, S. D. M., & Yahil, A. 1989, ApJ, 344, 1 (G89)
Groth, E. J., Juszkiewicz, R., & Ostriker, J. H. 1989, ApJ, 346, 558
Haynes, M. P., Giovanelli, R., Chamaraux, P., da Costa, L. N., Freudling, W., Salzer, J. J., & Wegner, G. 1999a, AJ, 117, 2039 (H99a)
Haynes, M. P., Giovanelli, R., Salzer, J. J., Wegner, G., Freudling, W., da Costa, L. N., Herter, T., & Vogt, N. P. 1999b, AJ, 117, 1668 (H99b)
Kaiser, N. 1988, MNRAS, 231, 149
Kolatt, T., & Dekel, A. 1996, ApJ, 479, 592
Liddle, A. R., Lyth, D. H., Schaefer, R. H., Shafi, Q., & Viana, P. T. P. 1996, MNRAS, 281, 531
Mathewson, D. S., Ford, V. L., & Buchhorn, M. 1992, ApJS, 81, 413
Monin, A. S., & Yaglom, A. M. 1975, Statistical Fluid Mechanics (Cambridge: MIT Press)
Peacock, J. A., & Dodds, S. J. 1994, MNRAS, 267, 1020
Peebles, P. J. E. 1980, The Large-Scale Structure of the Universe (Princeton: Princeton Univ. Press)
Sigad, Y., Dekel, A., Eldar, A., Strauss, M., & Yahil, A. 1998, ApJ, 495, 516
Strauss, M. A., Cen, R. Y., & Ostriker, J. P. 1993, ApJ, 408, 389
Strauss, M. A., & Willick, J. A. 1995, Phys. Rep., 261, 271
Tormen, G., & Bertschinger, E. 1996, ApJ, 472, 14
Tormen, G., Moscardini, L., Lucchin, F., & Matarrese, S. 1993, ApJ, 411, 16 (T93)
Watkins, R. 1997, MNRAS, 292, 59
Willick, J. A., Courteau, S., Faber, S. M., Burstein, A., Dekel, A., & Strauss, M. A. 1997, ApJS, 109, 333
Willick, J. A., & Strauss, M. A. 1998, ApJ, 507, 64
Zaroubi, S., Zehavi, I., Dekel, A., Hoffman, Y., & Kolatt, T. 1997, ApJ, 486, 21
Zehavi, I., Riess, A. G., Kirshner, R. P., & Dekel, A. 1998, ApJ, 503, 483
Zeldovich, Y. B. 1970, A&A, 5, 84